

Reducing the False Positive Rate Using Bayesian Inference in Autonomous Driving Perception

1st Johann J. S. Bastos

*Electrical Technical Coordination
Federal Institute of Espírito Santo
São Mateus, Espírito Santo, Brazil
jjakobschmitz@gmail.com*

2nd Bruno L. S. da Silva

*Electrical Technical Coordination
Federal Institute of Espírito Santo Santo
São Mateus, Espírito Santo Santo, Brazil
bruno.legora@ifes.edu.br*

3rd Tiago Zanotelli

*Electrical Technical Coordination
Federal Institute of Espírito Santo Santo
São Mateus, Espírito Santo Santo, Brazil
tiagoz@ifes.edu.br*

4th Cristiano Premebida

*Institute of Systems and Robotics
University of Coimbra
Coimbra, Portugal
cpremebida@isr.uc.pt*

5th Gledson Melotti

*Electrical Technical Coordination
Federal Institute of Espírito Santo Santo
São Mateus, Espírito Santo Santo, Brazil
gledson@ifes.edu.br (research coordinator)*

Abstract—Object recognition is a crucial step in perception systems for autonomous and intelligent vehicles, as evidenced by the numerous research works in the topic. In this paper, object recognition is explored by using multisensory and multimodality approaches, with the intention of reducing the false positive rate (FPR). The reduction of the FPR becomes increasingly important in perception systems since the misclassification of an object can potentially cause accidents. In particular, this work presents a strategy through Bayesian inference to reduce the FPR considering the likelihood function as a cumulative distribution function from Gaussian kernel density estimations, and the prior probabilities as cumulative functions of normalized histograms. The validation of the proposed methodology is performed on the KITTI dataset using deep networks (DenseNet, NasNet, and EfficientNet), and recent 3D point cloud networks (PointNet, and PintNet++), by considering three object-categories (cars, cyclists, pedestrians) and the RGB and LiDAR sensor modalities.

Index Terms—False Positive Rate, Bayesian Inference, Multi-modality, Deep networks, Perception systems, Object recognition

I. INTRODUCTION

Research on robotic perception has achieved very satisfactory results in terms of object recognition [1], [2], contributing significantly to the progress of autonomous and intelligent vehicles (AV/IV), due to technological advances such as hardware, sensors and statistical learning techniques. Perception systems for AV/IV can be understood as a process that interprets the data provided by the sensors in order to understand the surrounding environment, thus contributing to safer decision-making. An important item in perception systems is the object classification part, which is currently dominated by deep network (DN) architectures [3]–[6].

Frequently, the DNs present the confidence of the predictions as scores normalized between the values 0 and 1 by the softmax or sigmoid function [7], [8]. However, DNs do not always correctly classify the objects and the misclassified objects, which are defined as false positives (FPs), tend to have high score values. Thus, classification systems can have

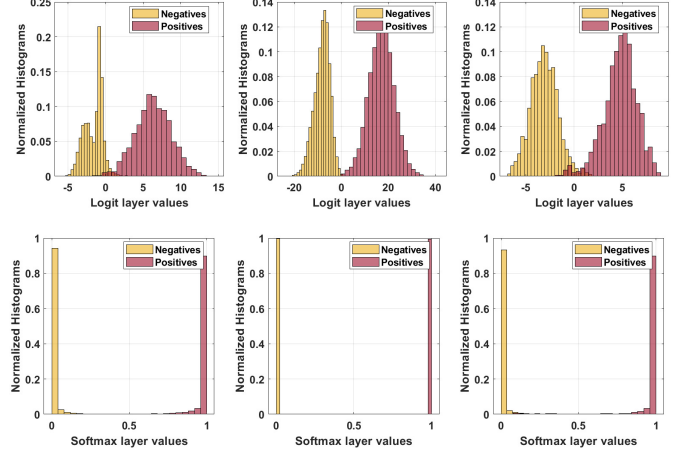


Fig. 1. Representations of distributions in normalized histograms (NH) of logit values in the 1st row, and the 2nd row the softmax values.

FPs with high-scores *i.e.*, high confidence, impairing decision-making by perception systems. On the other hand, the reduction of the FPR in classification systems would provide safer actions for decision-making, especially in relation to autonomous and intelligent vehicles.

An alternative to reduce the FPR can be through probabilistic interpretation by observing the logit layer values (score values before the prediction layer) [14]. Fig. 1 shows the distribution of logit values from an already trained network, in the first row, while the second row shows the distribution of the same scores after the softmax (SM). It is possible to see that the logit values are smoother than the softmax values *i.e.*, the values from softmax function are overconfident [10]–[13].

Softmax function (SM) is generally used as prediction function to classify a given input (decision-making) [9]. Such function can be taken in the probabilistic context by means of the Bayes' theorem, considering probabilistic generative models in classifications (Naive Bayes, Bayesian networks and

Hidden Markov Models) *i.e.*, the class-conditional densities and the prior are modeled, and then the posterior probabilities are computed through the Bayes' theorem. In other words, first we have to determine the class-conditional density (likelihood function) for each class individually and then the class prior probability. Equivalently, the joint distribution can be directly modeled and later normalized to obtain the posterior probability. In fact, the classification result is given through two stages, the first being inference (distribution modeling) and the second being decision-making (classification) [14].

Alternatively, many traditional approaches to classification problems are of the type called discriminative models (logistic regression and support vector machine) or discriminant functions (traditional neural networks and k-nearest neighbors). The first tries to model a posterior probability directly using a parametric model in the inference stage, and consequently optimizing such parameters through the training set. Given the posterior model, for each new entry, it assigns a top-class label. The second case *i.e.*, discriminant function, the approach defines a function which uses the training data to map each entry directly to a certain class (input-output mapping), and according to [14] the “probabilities play no role” *i.e.*, it is not possible to access posterior probabilities. In this case the inference and decision stages are into a single learning algorithm [14].

The result achieved by a machine learning algorithm, such as a classifier considering the prediction as the *SM*, should be carefully analyzed, so that the prediction result is not considered as a proper probabilistic value. To obtain adequate probabilistic results, the structure of the learning algorithms must encompasses probabilistic formulations.

In this context, this paper explores the well-known Bayes' theorem as a probabilistic interpretation of the predicted values from the logit values, through Maximum Likelihood (*ML*) and Maximum a-Posteriori (*MAP*) formulations. Additionally, we aim to reduce the false positive rate (*FPR*) without degrading the results already achieved by the neural networks. In fact, the *ML* and *MAP* formulations replace the predicted values of the neural network trained with the *SM* prediction function, without the need to retrain the neural network *i.e.*, the likelihood functions and prior probabilities of each class were obtained with the logit values (before *SM* prediction layer). The likelihood function is then defined by as a cumulative distribution function from the Gaussian kernel density estimation, and the prior probability as a cumulative function from of normalized histogram (*NH*), both with the logit layer values of already trained networks.

In summary, the contributions are:

- An investigation of the parametric and nonparametric modeling to represent the likelihood function and the prior probability, considering cumulative distribution functions;
- Reducing the *FPR* through Maximum likelihood and Maximum a-Posteriori formulations for object classification;

- A study with five different neural network architectures to validate the proposed approach, taking into account datasets from different modalities and sensors (RGB images, and 3D point clouds-LiDAR), contributing to advances in multisensory and multimodality perception.

II. RELATED WORK

There are many recent works that address False Positive Reduction techniques in different contexts, such as disease detection, security breach detection and vehicle detection. For the first context, the authors in [20] proposed a novel asymmetric residual network that uses 3D features and spatial information to improve classification and reduce false positives in lung nodule detection. Their network showed promising results in reducing false positive in clinical applications. In [21], the authors proposed a post-processing method to extract the confidence score of a prediction from a single channel of one layer of a Convolutional Neural Network (CNN) architecture. While using the confidence score of several layers of a CNN, their approach could reduce up to 18% of the false positive detection in one of their tests. The authors of [22] proposed a post-processing method to reduce false positives in lung cancer detection. Their method is lightweight and does not bring any constraints in the “front network”, while reducing 6.4% of the false discovery rate in their tests. In [23], the authors proposed a novel slice-fusion method with a Mask R-CNN detection model to reduce false positives in liver tumor detection. Their approach also improved the performance of tumor segmentation

Regarding the security breach context, the authors of [25] proposed a framework for addressing zero-day attacks in software (attacks that occur before the developer can take action on it), combining features selection methods and fine-tuning of their datasets. In [26], the authors proposed a technique to reduce false positives in hardware Trojan (HT) detection. Their method combines signal justification and unsupervised K-means, and is a general technique that can be applied to suspicious signals in detecting HT. Their experiments were done on various combinations of full and partial-scans of circuits, and obtained a false positive ratio of 3.89% and 3.31% for full and partial scans of circuits. In [24], an improved stacking ensemble algorithm was proposed to enhance the true positive rate of a intrusion detection system (IDS). Their Hybrid IDS was tested and their results showed that the method was superior than the compared techniques, in terms of True and False positives. In the software development context, the authors of [27] proposed a Transformer-based learning approach to identify false positive bug warnings found by static analysis tools, which usually return a large number of false positives that developers must verify manually. Their approach improved the precision of a tool by 17.5% and 5.5%, when considering *null dereferences* and *resource leaks* warnings, respectively.

Lastly, in the vehicle detection context, the authors of [29] proposed an asymmetric late fusion approach to fuse camera and LiDAR outputs from different networks. Their objective

was to eliminate false positives in these object detectors. According to their results, their objective was reached and the method achieved up to 9.87% better class-wise performance than the LiDAR-only detector. In [28], two end-to-end trainable feature fusion techniques were proposed to combine RGB and point-cloud features. Their experiments showed that their methods can improve significantly the filtering of false positive from data. Their approaches can be applied to improve the false positive ratio in many different architectures.

III. PROPOSED METHOD

A. Probabilistic Inference

This section presents the formulations to reduce *FPR*, through Maximum Likelihood (*ML*) and Maximum a-Posteriori (*MAP*) functions, based on the Bayes' rule (1), including nonparametric and parametric modeling to define the posterior probability, likelihood function, and prior probability as well. Expressing the posterior by

$$P(\mathbf{C}|\mathbf{Sc}) = \frac{P(\mathbf{Sc}|\mathbf{C})P(\mathbf{C})}{P(\mathbf{Sc})}, \quad (1)$$

where \mathbf{C} is the random variable (rv) associated to the object categories, \mathbf{Sc} ¹ are the classified object scores (predicted values), $P(\mathbf{Sc}|\mathbf{C})$ is the likelihood, $P(\mathbf{C})$ is the prior probability and $P(\mathbf{Sc}) \neq 0$ is the model evidence, considering the prior and likelihood are known. From the law of the total probability [14], (1) can be rewritten using the *per-class* expression,

$$P(c_i|\mathbf{Sc}) = \frac{P(\mathbf{Sc}|c_i)P(c_i)}{\sum_{i=1}^{nc} P(\mathbf{Sc}|c_i)P(c_i)}, \quad (2)$$

where $P(\mathbf{Sc}|c_i)$ is the likelihood of an object for the class (c_i). Given (2), an inference can be made on the test set about the “unknown” rv \mathbf{C} from the dependence with \mathbf{Sc} *i.e.*, the value of the posterior distribution of \mathbf{C} is determined after observing the value of \mathbf{Sc} [12], [12], [13].

B. ML and MAP Functions

Often, the values from the logit layer are more suitable for representing a probability density function, when compared with the values of the *SM* function, as illustrated by the distributions in Fig. 1. Thus, from (2) we can define the Maximum Likelihood and the Maximum a-Posteriori function, as (3) and (4) respectively [12], [12], [13] thus,

$$ML := \arg \max_i \frac{(P(\mathbf{Sc}|c_i) + \lambda)}{\sum_{i=1}^{nc} (P(\mathbf{Sc}|c_i) + \lambda)}, \quad (3)$$

$$MAP := \arg \max_i \frac{(P(\mathbf{Sc}|c_i)P(c_i) + \lambda)}{\sum_{i=1}^{nc} (P(\mathbf{Sc}|c_i)P(c_i) + \lambda)}, \quad (4)$$

where λ represents the additive smoothing parameter, used here to avoid the zero probability problem [15].

¹Generally, neural network score values are obtained using a prediction function that normalizes logit values between zero and one, such as the softmax prediction function.

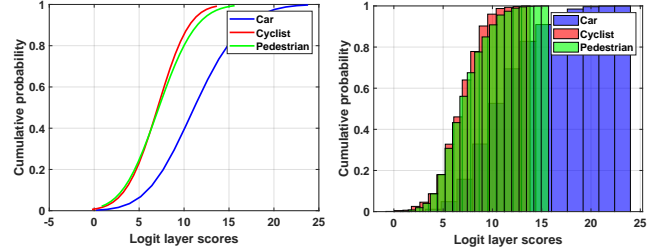


Fig. 2. CDF representations obtained from Gaussian functions (first column) and normalized histograms (second column).

C. Kernel Density Estimation and Normalized Histogram

We propose to model the *ML* and *MAP* functions, which will perform the inference, by taking the cumulative distribution function (CDF), where the density is extracted by using the logit layer values (before softmax prediction layer values) from the training set data, as illustrated in Fig. 2.

Note that the graphics on the left of Fig. 2 represents CDFs modelled by Gaussians (likelihood functions) *i.e.*, they are modeled using parametric estimates by means of a Kernel Density Estimation (KDE) given in (5), which computes the average of several probability density function to obtain a kernel estimate of the probability density function [12], [16], [17].

$$\hat{f}_{ker}(d) = \frac{1}{nh} \sum_{i=1}^n K\left(\frac{d - Sc_i}{h}\right), \quad (5)$$

where h is a smoothing parameter² called window width or bandwidth (bw)³, n is the number of observations, d is a value set⁴ (domain) that evaluates the function $\hat{f}_{ker}(d)$, Sc_i are the predicted values (scores) of each object classified to a certain class, $K\left(\frac{d - Sc_i}{h}\right) = K(t)$ is the kernel, having the condition that $\int K(t)dt = 1$ to ensure that the estimate in (5) is a proper probability density function. Such function is computed at each data point and then taking the average of them. The kernel and the estimated function are defined according to the (5), and (6),

$$K(t) = \frac{1}{\sqrt{2\pi}} e^{-\frac{t^2}{2}} \Rightarrow \hat{f}_{ker}(d) = \frac{1}{nh} \sum_{i=1}^n \frac{1}{\sqrt{2\pi}} e^{-\left(\frac{1}{2h^2}\right)(d - Sc_i)^2} \quad (6)$$

where $t = \frac{d - Sc_i}{h}$, and each kernel function is evaluated at d centered at data Sc_i [12].

The idea of applying Gaussian functions is to obtain a smoother data distribution, as shown in Fig. 1 (1st row). In other words, the distribution from the logit layer is more suitable for modeling a probability density function. Furthermore, the normal (Gaussian) distribution has a maximum entropy *i.e.*, a distribution with more information and less confident information around the mean (distribution with high variance) [13], [14].

²This smoothing parameter is not related to the smoothing parameter of Bayesian inference functions (*ML* and *MAP*).

³Small values generate rough curves, while larger values generate smoother curves.

⁴The d values are not related to the values of scores or logits.

Algorithm 1: compute the estimated cumulative density function.

Input

- Data Sc_i ;
- d is the set of values to evaluate \hat{f}_{ker} ;
- h is the window width (bandwidth);
- kernel function defined as probability density function.

Output

- Cumulative density function (CDF) is calculated from the average of the estimated probability density functions.

$f_{hat} \leftarrow zeros(size(d))$; /* take the average of weighted curves */

for $k \leftarrow 1 : n$ **do**

$$f \leftarrow \frac{1}{\sqrt{2\pi}} e^{-\left(\frac{1}{2h^2}\right)*(d-Sc_i)^2}$$

$f \leftarrow f/h$ /* weight each curve by $1/h$ */

$f_{hat} \leftarrow f_{hat} + f/n$ /*a weighted sum (1/h) of the kernel function value at each value of d */

end

$$CDF \leftarrow \sum_{Sc_i \leq Sc} f_{hat}(Sc_i)$$

Prior probabilities are represented by CDFs obtained from normalized histograms (NH), as illustrated on the right of Fig 2. According to [17] “A histogram is a way to graphically represent the frequency distribution of a data set. Histograms are a good way to *i*) summarize a data set to understand general characteristics of the distribution such as shape, spread, or location; *ii*) suggest possible probabilistic models, *iii*) or determine unusual behavior”. In other words, here the NH is used to model proper distributions. The histogram is constructed from the number of bins (intervals) *i.e.*, the number of bars, which must not overlap with each other and the bins should have the same width [12].

In an implementation perspective, the formulation to get $P(\mathbf{Sc}|c_i)$ for the ML function can be computed as illustrated in Fig. 3, while the MAP function (posterior probability) follows what is illustrated in Fig. 4. Therefore, the ML and MAP functions replace the softmax function only on the test data, using the logit layer values, while the CDFs were obtained with the logit data from the training dataset. Notice that, although the Bayesian formulation takes distributions into account, ML and MAP compute a single estimate rather than a distribution.

The use of different models to represent the distributions aims to capture different information from the training data. The choice of obtaining a CDF from a Gaussian distribution to represent the likelihood function and a CDF from NH to represent the prior probability were defined based on preliminary experiments. The reverse could be valid *i.e.*, a Gaussian distribution for the likelihood function and NH for the prior probability.

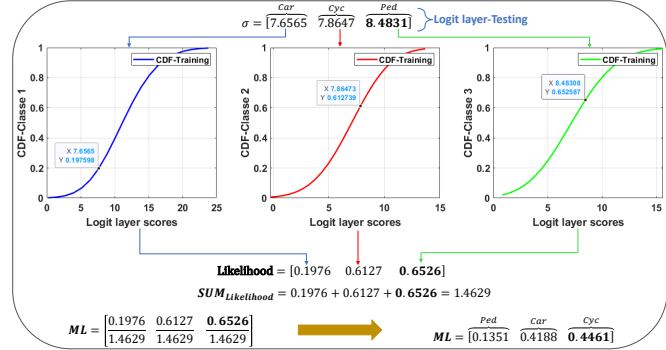


Fig. 3. The likelihood function ($P(\mathbf{Sc}|c_i)$) is calculated per class for each classified object *i.e.*, the ML .

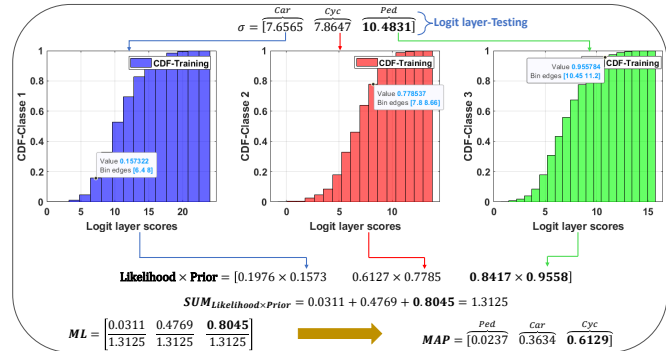


Fig. 4. The prior probability ($P(c_i)$) is computed per class for each classified object, as well as the MAP .

D. Setting the KDE and NH Parameter

KDE’s formulation involves determining h *i.e.*, the smoothing parameter for each class, according to a (6). Differently, the NH is constructed using the number of bins ($nbins$) for each class. Thus, the determination of such parameters was obtained through a genetic algorithm optimization⁵, considering in the cost function the F-score (F1) and FPR , as defined in (7),

$$F_{cost} = \min[(1 - F1) + FPR]. \quad (7)$$

The optimization process of the genetic algorithm was carried out with the training data and validated on the validation data, for the determination of the KDE and NH parameters *i.e.*, the parameters that provide the lowest value for FPR and the highest value for the F-score.

Note that this paper aims to reduce the rate of false positives without degrading the classification results, in other words, without degrading the results of the F-score metric: this is the reason of using the F-score in the cost function of the genetic algorithm.

E. Dataset

To validate the proposed methodology, this paper considers three neural networks that process RGB images (DenseNet [30], NasNet [31], and EfficientNet [32]) and two neural network that directly processes 3D point clouds (PointNet [33], and PointNet++ [34]). The results were achieved

⁵In this work, the Matlab genetic algorithm toolbox was used.

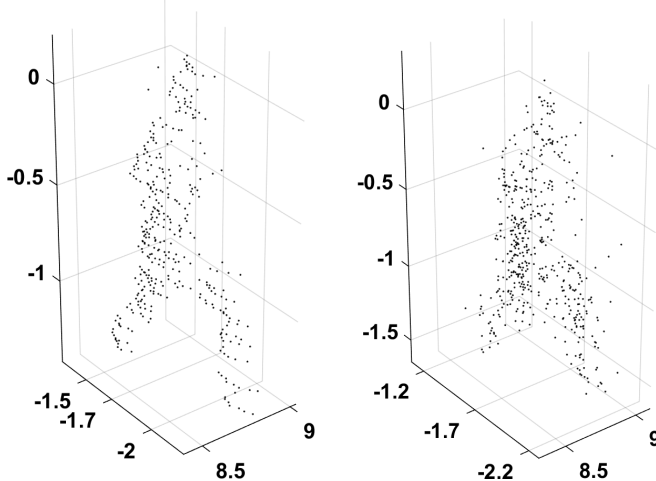


Fig. 5. The pedestrian on the left contains the number of original points of the frame (364 points), on the right the same pedestrian with 512 points (upsample). The axis are shown in meters.

TABLE I

KITTI DATASET FOR CLASSIFICATION: NUMBER OF OBJECTS PER CLASS AND AND RESPECTIVE SUBSETS.

RGB Images - 7481 Frames			
	Car	Cyclist	Pedestrian
Training	18103	1025	2827
Validation	2010	114	314
Testing	8620	488	1346
3D Point Clouds - 7481 Frames			
	Car	Cyclist	Pedestrian
Training	15324	923	2688
Validation	1717	99	303
Testing	7332	452	1260

using the KITTI Object Detection dataset, where the objects have been extracted (cropped) both from the RGB image frames and from the 3D point clouds frames. The 3D point clouds objects contain different amount of points because of the nature of the 3D LiDAR sensor. Thus, some objects had the amount of points reduced to 512 points (random downsample) or increased to 512 points (considering the k nearest neighbors), as shown in Fig. 5. The process of cropping the 3D points is described in [12], [18], [19]. Table I shows the number of objects for images and point clouds.

IV. EXPERIMENTS AND RESULTS

Assessing the false positive rate (FPR) in real world applications is relevant in autonomous drive scenarios, since objects can be misclassified by prediction functions in neural networks with high score values. In this section we evaluated (on a test set *i.e.*, prediction stage) the proposed approaches by replacing the *SM* by the *ML* and *MAP* prediction functions, considering the likelihood as CDFs from Gaussian functions, and prior probabilities are represented by CDFs obtained from NH as described in Sect.III.

Results achieved on the classification test set are shown in Table II, in terms of FPR and F-score performance measures. It can be seen that the FPR decreased after replacing the *SM* function with the *ML* and *MAP* functions. Regarding the RGB image classifications, particularly with the EfficientNet

network, the FPR decreased significantly, given that the reduction is 25.63% for *ML* and 15.34% for *MAP*. On the other hand, the values of the F-scores decreased very slightly in almost all networks (although this did not compromise the classification performance), with the exception of the NasNet network that increased the value of the F-score using the *MAP* function - which is very positive. Another significant FPR reduction occurred with the PointNet network, achieving a value of 16.98% reduction when using the proposed *ML* function. The parameters (*nbins*, λ , and *bw*) determined by the genetic algorithm are presented in the tables III, IV, and V.

Finally, it is worth mentioning that this paper is not concerned about which classification network is the best in terms of performance but, rather a study of FPR reduction *i.e.*, the efficiency of the proposed methodology in deep networks that can potentially be employed as part of perception systems.

V. CONCLUDING REMARKS

The techniques and experimental results described in this paper are based on a proposed probabilistic approach that uses density distributions to model the networks logit values *i.e.*, the top-class scores before the softmax prediction layer. The results reported in this work are very promising, given that *ML* and *MAP* reduced the FPR of the deep models without the need to retrain the neural networks, while the F-score metric achieved a very small reduction which means the overall classification performance was not compromised.

A potential way to improve the results of the F-score metric by the *ML* and *MAP* functions could be by adjusting the internal parameters of the genetic algorithm (mutation rate, population size, crossover rate, etc.), as well as modifying the cost function of such algorithm.

Finally, a potentially significant aspect that contributed to validate the proposed approach was the use of distinct modalities and sensors, considering RGB images (camera sensor) and 3D point clouds (LiDAR).

REFERENCES

- [1] Wang, C., Yuan, J., Xie, L.: Non-iterative slam, 18th International Conference on Advanced Robotics (ICAR), pp. 83–90, (2017).
- [2] Siritanawan, P., Prasanjith, M. D., Wang, D.: 3D feature points detection on sparse and non-uniform pointcloud for slam”, 18th International Conference on Advanced Robotics (ICAR), pp. 112–117, (2017).
- [3] Singh, G., et al.: ROAD: The road event awareness dataset for autonomous driving, IEEE Trans. Pattern Anal. Mach. Intell., 45(1), pp. 1036–1054, (2023).
- [4] Liao, Y., Xie, J., Geiger, A.: KITTI-360: A novel dataset and benchmarks for urban scene understanding in 2D and 3D, IEEE Trans. Pattern Anal. Mach. Intell., 45(3), pp. 3292–3310, (2023).
- [5] He, Q., Wang, Z., Zeng, H., Zeng, Y., Liu, Y., Liu, S., Zeng, B.: Stereo RGB and deeper LiDAR-based network for 3D object detection in autonomous driving, IEEE Trans. Intell. Transp. Syst., 24(1), pp. 152–162, (2023).
- [6] Janai, J., et al.: Computer vision for autonomous vehicles: Problems, datasets and state of the art, Foundations and Trends in Computer Graphics and Vision, Now Publishers Inc, 12(1-3), (2020).
- [7] Su, D., Zhang, H., Chen, H., Yi, J., Chen, PY., Gao, Y.: Is robustness the cost of accuracy? A comprehensive study on the robustness of 18 deep image classification models, 15th European Conference on Computer Vision, Springer International Publishing, Springer, Cham, pp. 644–661, (2018).

TABLE II

COMPARISON BETWEEN THE CLASSIFICATIONS OBTAINED BY THE *SM*, *ML* AND *MAP* FUNCTIONS IN TERMS OF AVERAGE F-SCORE AND *FPR* (%).

Prediction Function	DenseNet		NasNet		EfficientNet		PointNet		PointNet++	
	<i>FPR</i> ↓	F-score ↑	<i>FPR</i> ↓	F-score ↑	<i>FPR</i> ↓	F-score ↑	<i>FPR</i> ↓	F-score ↑	<i>FPR</i> ↓	F-score ↑
<i>SM</i>	0.7202	97.38	0.7202	96.98	0.4545	98.44	5.36	80.39	2.66	92.51
<i>ML_{KDE}</i>	0.6788	97.09	0.7146	96.81	0.3380	98.14	4.45	80.30	2.31	92.17
<i>MAP_{KDE}</i>	0.7122	96.52	0.7026	97.08	0.3848	98.32	4.49	80.10	2.35	92.03

TABLE III

PARAMETER VALUES FOR KDE *i.e.*, THE VALUES OF *h* (*bw*) FOR EACH CLASS, AS WELL AS THE VALUE OF λ IN THE *ML* FORMULATION.

Neural Network	Parameter			
	<i>h_{Car}</i>	<i>h_{Cyc}</i>	<i>h_{Ped}</i>	λ
DenseNet	2.24	1.29	1.90×10^{-1}	5.56×10^{-7}
NasNet	2.89	4.95×10^{-1}	5.46×10^{-1}	2.13×10^{-7}
EfficientNet	2.02	2.35	1.25	8.48×10^{-7}
PointNet	2.33	0.18	2.85	8.62×10^{-7}
PointNet++	1.54	0.87	2.53	6.66×10^{-7}

TABLE IV

PARAMETER VALUES FOR KDE *i.e.*, THE VALUES OF *h* (*bw*) FOR EACH CLASS, AS WELL AS THE VALUES OF THE NUMBER OF BINS (*nbins*) USED FOR THE NHs AND λ IN THE *MAP* FORMULATION.

Neural Network	Parameter			
	<i>h_{Car}</i>	<i>h_{Cyc}</i>	<i>h_{Ped}</i>	λ
DenseNet	2.50	1.24	1.20	1×10^{-8}
NasNet	2.48	8.81×10^{-2}	9.96×10^{-2}	3.99×10^{-7}
EfficientNet	2.65	1.49	1.85	1.51×10^{-7}
PointNet	2.51	0.55	2.51	1.80×10^{-7}
PointNet++	2.55	0.23	2.90	1.34×10^{-7}

TABLE V

PARAMETER VALUES FOR THE NUMBER OF BINS (*nbins*) OF THE HISTOGRAMS IN THE *MAP* FORMULATION.

Neural Network	Parameter		
	<i>nbins_{Car}</i>	<i>nbins_{Cyc}</i>	<i>nbins_{Ped}</i>
DenseNet	3	3	3
NasNet	4	42	40
EfficientNet	17	29	17
PointNet	7	39	4
PointNet++	32	25	5

- [8] Bochkovskiy, A., Wang, C-Y., Liao, H-Y. M.: OLOv4: Optimal speed and accuracy of object detection, arXiv:2004.10934, (2020).
- [9] Patra, R., Hebbalaguppe, R., Dash, T., Shroff, G., Vig., L.: Calibrating deep neural networks using explicit regularisation and dynamic data pruning, in Proc. IEEE Winter Conf. Appl. Comput. Vis. (WACV), pp. 1541–1549, (2023).
- [10] Guo, C., Pleiss, G., Sun, Y., Weinberger, K.Q.: On calibration of modern neural networks, in Proc. 34th Int. Conf. Mach. Learn., vol. 70, pp. 1321–1330, (2017).
- [11] Pereyra, G., Tucker, G., Chorowski, J., Kaiser, L., Hinton, G.: Regularizing neural networks by penalizing confident output distributions, arXiv:1701.06548, (2017).
- [12] Melotti, G., et al.: Probabilistic Approach for Road-Users Detection, in IEEE Transactions on Intelligent Transportation Systems, pp. 1–15, (2023).
- [13] Melotti, G., Premebida, C., Bird, J.J., Faria, D.R., Gonçalves, N.: Reducing Overconfidence Predictions in Autonomous Driving Perception, in IEEE Access, vol. 10, pp. 54805–54821, (2022).
- [14] Bishop, C. M.: Pattern Recognition and Machine Learning. Cham, Switzerland: Springer, (2006).
- [15] Valcarce, D., Parapar, J., Barreiro.: Additive smoothing for relevance-based language modelling of recommender systems, in Proc. 4th Spanish Conf. Inf. Retr., pp. 210–216, (2016).
- [16] Scott, D. W.: Multivariate density estimation : theory, practice, and visualization. Wiley series in probability and mathematical statistics. Wiley, (1992).
- [17] Martinez, W.L., Martinez, A.R.: Computational Statistics Handbook with MATLAB, 3rd ed., Chapman and Hall/CRC, (2015).
- [18] Melotti, G., Premebida, C., Gonçalves, N.: Multimodal Deep-Learning for Object Recognition Combining Camera and LIDAR Data, IEEE International Conference on Autonomous Robot Systems and Competitions, pp. 177–182, (2020).
- [19] Melotti, G., Asvadi, A., Premebida, C.: "CNN-LIDAR pedestrian classification: combining range and reflectance data," IEEE International Conference on Vehicular Electronics and Safety, pp. 1-6, (2018).
- [20] Liu, B., Song, H., Li, Q., Lin, Y., Weng, X., Su, Z., Yang, J.: 3D ARCNN: An Asymmetric Residual CNN for False Positive Reduction in Pulmonary Nodule, in IEEE Transactions on NanoBioscience, pp. 1644–1647, (2023).
- [21] Vasiliuk, A. and Belyaev, M.: Reducing False-Positive Detections Using the Distance Between Activation Distributions in Individual Channels, in Ural-Siberian Conference on Biomedical Engineering, Radioelectronics and Information Technology, pp. 016–019, (2022).
- [22] Mai , J., et al.: MHSnet: Multi-head and Spatial Attention Network with False-Positive Reduction for Lung Nodule Detection, in IEEE International Conference on Bioinformatics and Biomedicine, pp. 1108–1114, (2022).
- [23] Tu, D. Y., Lin, P. C., Chou, H. H., Shen, M. R., Hsieh, S. Y.: Slice-Fusion: Reducing False Positives in Liver Tumor Detection for Mask R-CNN, in IEEE Trans. on Computational Biology and Bioinformatics, pp. 1–11, (2023).
- [24] Yin, B., Bu,B., Gao, B., Li, Q.: A Hybrid Intrusion Detection Method using Improved Stacking Ensemble Algorithm and False Positive Elimination Strategy for CBTC, in IEEE 25th International Conference on Intelligent Transportation Systems, pp. 4253–4258, (2022).
- [25] Pitre, P. and Gandhi, A., Konde, V., Adhao, R., Pachghare, V.: An Intrusion Detection System for Zero-Day Attacks to Reduce False Positive Rates, International Conference for Advancement in Technology, pp. 1–6, (2022).
- [26] Salmani, H.: Gradual-N-Justification (GNJ) to Reduce False-Positive Hardware Trojan Detection in Gate-Level Netlist, in IEEE Transactions on Very Large Scale Integration Systems, pp. 515–525, (2022).
- [27] Kharkar, A., et al.: Learning to Reduce False Positives in Analytic Bug Detectors, in IEEE/ACM 44th International Conference on Software Engineering, pp. 1307–1316, (2022).
- [28] Z. Zhang et al., MAFF-Net: Filter False Positive for 3D Vehicle Detection with Multi-modal Adaptive Feature Fusion, in IEEE 25th International Conference on Intelligent Transportation Systems, pp. 369–376, (2022).
- [29] Çaldıran, B. E., Acarman, T.: A Late Asymmetric Fusion Approach To Eliminate False Positives, in IEEE 25th International Conference on Intelligent Transportation Systems, pp. 2080–2085, (2022).
- [30] Huang, G., Liu, Z., Van Der Maaten, L., Weinberger, K.Q.: Densely Connected Convolutional Networks, IEEE Conference on Computer Vision and Pattern Recognition, pp. 4700–4708, (2017).
- [31] Zoph, B., Vasudevan, V., Shlens, J., Le, Q.V.: Learning Transferable Architectures for Scalable Image Recognition, in IEEE Conference on Computer Vision and Pattern Recognition, pp. 8697–8710, (2018).
- [32] Tan, M., Le, Q.: EfficientNet: Rethinking Model Scaling for Convolutional Neural Networks, Proceedings of the 36th International Conference on Machine Learning, pp. 6105–6114, (2019).
- [33] Qi, C. R., Su, H., Kaichum, M., Guidas,L. J.: PointNet: Deep Learning on Point Sets for 3D Classification and Segmentation, Proceedings of the IEEE Conference on Computer Vision and Pattern Recognition, pp. 652–660, (2017).
- [34] Qi, C.R., Yi, L., Su, H., Guibas, L.J.: PointNet++: Deep Hierarchical Feature Learning on Point Sets in a Metric Space, Advances in Neural Information Processing Systems, vol. 30, (2017).